1-1-2007

Low-temperature synthesis of polypyrrole-coated LiV3O8 composite with enhanced electrochemical properties

Sau Yen Chew
University of Wollongong, syc410@uow.edu.au

Chuanqi Feng
Hubei University, China, cfeng@uow.edu.au

See How Ng
University of Wollongong, shn076@uow.edu.au

Jiazhao Wang
University of Wollongong, jiazhao@uow.edu.au

Zaiping Guo
University of Wollongong, zguo@uow.edu.au

See next page for additional authors

Journal of The Electrochemical Society, **154** (7) A633-A637 (2007)
0013-4651/2007/154(7)/A633/5/$20.00 © The Electrochemical Society

Low-Temperature Synthesis of Polypyrrole-Coated LiV_3O_8 Composite with Enhanced Electrochemical Properties

Sau Yen Chew,[a,b,*,z] Chuanqi Feng,[a,c] See How Ng,[a,b,*] Jiazhao Wang,[a,b] Zaiping Guo,[a,b] and Huakun Liu[a,b,]**

[a]*Institute for Superconducting and Electronic Materials, and* [b]*ARC Center of Excellence for Electromaterials Science, University of Wollongong, Wollongong, New South Wales 2522, Australia*
[c]*Department of Chemistry and Chemical Engineering, Hubei University, Wuhan 430062, China*

A composite, LiV_3O_8-polypyrrole (PPy), was synthesized by a low-temperature solution route followed by an in situ polymerization method. The as-prepared powders consisted of nanosized PPy distributed homogeneously within the layered lithium trivanadate. The electrochemical properties of LiV_3O_8–PPy composite were systematically investigated and compared with bare lithium trivanadate. It was found that the electrochemical performance of the LiV_3O_8–PPy composite was significantly enhanced, with a specific capacity of $\sim$183 mAh g^{-1} retained after 100 cycles. This suggests that nanostructured PPy could work well as a polymer-conducting matrix and also as a binding material to improve the overall electrochemical properties of the LiV_3O_8 when used as a cathode material in lithium-ion batteries.
 [DOI: 10.1149/1.2734778]

Manuscript submitted December 21, 2006; revised manuscript received February 5, 2007. Available electronically May 9, 2007.

Lithium-ion batteries, which offer a higher operating voltage and energy density, are key devices in today's portable electronic society. Commercial lithium-ion cells use lithium cobalt oxide cathodes, and the high cost and low capacity of cobalt has prompted the design and synthesis of alternate insertion hosts. Intensive effort has been focused on the various kinds of inorganic metal oxides, in particular the layered oxides, $Li_xM_yO_z$, (M: V, Mn, Co, etc.), to improve the performance of the electrode materials.[1,2]

Layered lithium trivanadate, LiV_3O_8, has received considerable attention as a promising cathode material for rechargeable lithium batteries because of certain attractive properties, such as high specific capacity, easy preparation, and stability in air.[3,4] According to Nassau and Murphy,[4] the electrochemical performance, such as discharge capacity, rate capability, and cycle life of LiV_3O_8, are strongly influenced by the preparation method. Many methods have been applied to fabricate LiV_3O_8 particles, mainly the sol-gel method, rapid cooling, efficient grinding, hydrothermal synthesis, the dehydration method using aqueous lithium vanadate gel, microwave-assisted synthesis, and ultrasonic treatment.[5-12]

However, the electrical conductivity and viscosity of these oxide powders are extremely low. Therefore, the use of a conducting network and a binder is necessary in order to overcome these drawbacks. In general, carbon black and polyvinylidene fluoride (PVDF) are mixed with LiV_3O_8 to solve the problem, but the addition of materials without electrochemical activity reduces the apparent energy density.[13,14]

As is well known, polypyrrole (PPy) is the most popular conducting polymer with the ability to store electric charges, and it also works well as a binder.[13-18] The high electrical conductivity and electrochemical activity of PPy composites have been extensively studied, such as MnO_2–PPy,[13] $LiMn_2O_4$–PPy,[14] V_2O_5–PPy,[15] sulfur–PPy,[16] and $LiFePO_4$–PPy,[17] and their possibilities in the field of charge storage devices have also been pointed out. To the best of our knowledge, the synthesis of PPy-coated LiV_3O_8 composite for use in lithium-ion batteries has not been reported yet. Herein, a low-temperature route is applied to synthesize highly homogeneous, uniformly dispersed, and structurally disordered LiV_3O_8 particles. The PPy-coated LiV_3O_8 composite was prepared by an in situ oxidative polymerization of pyrrole around LiV_3O_8 particles. The structural characterization and electrochemical performance of LiV_3O_8–PPy composite are discussed and compared with the bare LiV_3O_8 material.

* Electrochemical Society Student Member.
** Electrochemical Society Active Member.
z E-mail: syc410@uow.edu.au

Experimental

Materials synthesis.— Lithium trivanadate, LiV_3O_8, was prepared by a low-temperature, rheological phase reaction.[10] The starting materials were analytically pure $LiOH{\cdot}H_2O$ (Aldrich), V_2O_5 (99%, Aldrich), and citric acid (>99% Sigma-Aldrich). First, stoichiometrically weighed amounts of $LiOH{\cdot}H_2O$, V_2O_5, and citric acid (1:1.5:4.8) were mechanically mixed in an agate mortar. A limited amount of distilled water was then added to the ground mixture to form a solid-liquid rheological phase. The mixture was then heated at 100°C for 12 h in a vacuum oven to evaporate the water, and a dark green precursor was obtained. Subsequently, the precursor was transferred to a porcelain crucible and sintered at 480°C for 12 h. A dark brown material was obtained.

LiV_3O_8–PPy composites were synthesized by an in situ oxidative polymerization method with sodium p-toluenesulfonate (PTSNa) as the dopant and $FeCl_3$ as the oxidant. The pyrrole was purified by distillation under atmospheric pressure prior to use. LiV_3O_8 (1.0 g) was dispersed into a 100 mL solution containing 0.013 mol dm^{-3} PTSNa and 0.038 mol dm^{-3} pyrrole. The mixture was magnetically stirred while 50 mL of 0.24 mol dm^{-3} $FeCl_3$ solution was slowly injected into the aqueous solution. It was observed after injecting $FeCl_3$ that the color of the mixture changed from dark brown to black, indicating the deposition of PPy on the surface of the oxide particles. Stirring of the reaction mixture was maintained for 20 h. The LiV_3O_8–PPy particles were separated from the mixture via centrifugation at 4400 rpm for 1 h, then washed several times with distilled water and, finally, dried under vacuum at 60°C for 4 h.

Composition and structure determination.— The precursor was analyzed by thermogravimetric and differential thermal analyses (TGA/DTA) via Setaram 92 equipment to verify the sintering temperature. Precise PPy contents in the nanocomposites were determined by TGA. The powders were characterized by X-ray diffraction (XRD) using a Philips PW1730 diffractometer with Cu Kα radiation and a graphite monochromator. Powder morphologies were investigated using a JEOL JSM 6460A scanning electron microscope (SEM).

Electrode preparation and coin-cell assembly.— The cathode was prepared by mixing LiV_3O_8 or LiV_3O_8–PPy composites as active materials with 10 wt % carbon black and 5 wt % polyvinylidene fluoride (PVDF) binder in *N*-methyl-2-pyrrolidinone (NMP) solvent to form a homogeneous slurry, which was then spread onto aluminium foil to form the electrodes. The coated electrodes were dried in a vacuum oven at 100°C for 24 h and then compressed at a pressure of 150 kg cm^{-2}. The electrochemical char-

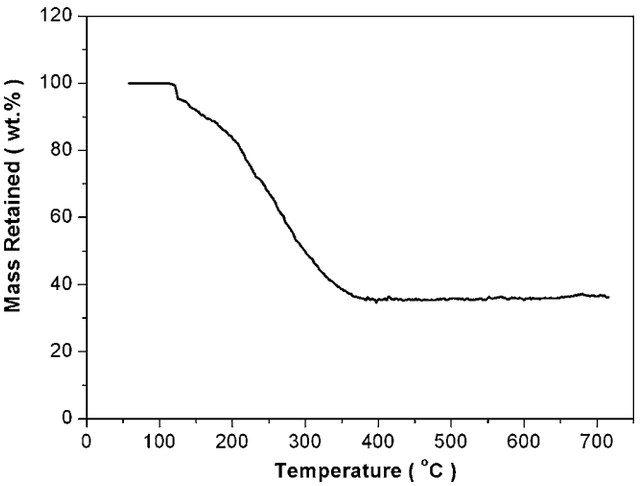

Figure 1. TGA curve of the LiV_3O_8 precursor.

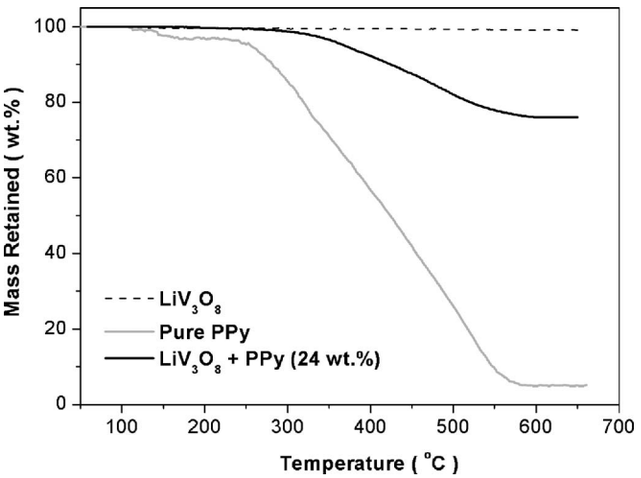

Figure 2. TGA curves of LiV_3O_8–PPy composite

acterizations were carried out using coin cells. CR 2032 coin-type cells were assembled in an argon-filled glove box (Mbraun, Unilab, Germany) by stacking a porous polypropylene separator between the electrode and a lithium foil counter electrode. The electrolyte used was 1 M $LiPF_6$ in a 50:50 (w/w) mixture of ethylene carbonate (EC) and dimethyl carbonate (DMC), provided by Merck KgaA, Germany.

Electrochemical measurements.— The cells were galvanostatically charged and discharged between 1.50 and 3.85 V at a constant current density of 40 mA g^{-1} at room temperature, using a Neware battery tester. The ac impedance spectroscopy was obtained by applying a sine wave of 5 mV amplitude over a frequency range of 100.00 kHz to 0.01 Hz using a CHI 660B electrochemical workstation system (CH Instrument, Cordova, TN).

Results and Discussion

TGA analysis of the precursor.— Figure 1 shows the TGA curve of the precursor, which was synthesized by the low-temperature solution route. The samples were heated from 60 to 700°C at a rate of 10°C min^{-1} in air. It can be observed that a weight loss of approximately 64% occurred between 115 and 400°C. Above 400°C, the amount of the reactant remained stable. Based on this result, the expected compound could be obtained by heating the precursor to 480°C.

Estimation of the amount of PPy in the LiV_3O_8–PPy composite.— To quantify the amount of PPy in the LiV_3O_8–PPy composite, TGA analysis was carried out. Figure 2 shows the TGA analysis of the LiV_3O_8–PPy composite along with those of bare LiV_3O_8 and PPy powders when heated from 60 to 650°C. Bare PPy powder burns off at 600°C, while the bare LiV_3O_8 powder maintains a constant weight in the temperature range used for this experiment. LiV_3O_8–PPy composite shows a single-step weight loss at a temperature of ~600°C, which corresponds to the burning of PPy. There is no further weight loss after the initial decomposition of PPy. Therefore, the change in weight before and after the burning of PPy directly translates into the amount of PPy in the LiV_3O_8–PPy composite. Using this method, it was found that the amount of PPy in the composite is 24 wt %.

Structure and morphology analysis of LiV_3O_8–PPy composite.— The XRD pattern (Fig. 3) of as-prepared LiV_3O_8 was collected between 2Θ angles of 10 and 60° at a scan rate of 2 deg min^{-1}. The diffraction peak positions for the sample are consistent with the known layered-type LiV_3O_8 lattice constants given in the literature as a = 6.68 Å, b = 3.60 Å, and c = 12.03 Å (JCPDS 72-1193). On the basis of the peak broadening observed in LiV_3O_8, when the Debye–Scherrer equation was applied to the (100) peak, it indicated a crystallite size of ~50 nm. This phenomenon has also been reported in the literature, which indicates that the dimensions of the materials are relatively small and fine in nature, with isotropic and strain-free crystallites.[6,8,19] The peak at about 14° is assigned to diffraction at the (100) plane, indicating the layered structure of LiV_3O_8. These layers consist of VO_6 octahedra and VO_5 trigonal bipyramids, which are corner sharing with the octahedra. The Li cations are assumed to be intercalated between such layers.[5,20] Figure 3 also revealed that the XRD pattern of LiV_3O_8–PPy composite is similar to that of LiV_3O_8. No obvious diffraction peaks due to impurity phases were observed.

From SEM images (Fig. 4a), it can be observed that the layered host LiV_3O_8 consists of flakelike agglomerates with sharp edges. By comparison, LiV_3O_8–PPy composite presents a distinct contrast in the morphology (Fig. 4b), which confirms the coexistence of two phases, i.e., amorphous PPy and LiV_3O_8 particles. The nanosized PPy are well dispersed in the LiV_3O_8 particles. The size of the PPy particles ranges from below 80 to ~ 200 nm (Fig. 4c).

To verify the homogeneity of PPy distribution in the LiV_3O_8 particles, energy-dispersive X-ray (EDX) mapping of different elements was conducted (Fig. 5). The bright spots shown in Fig. 5b-d

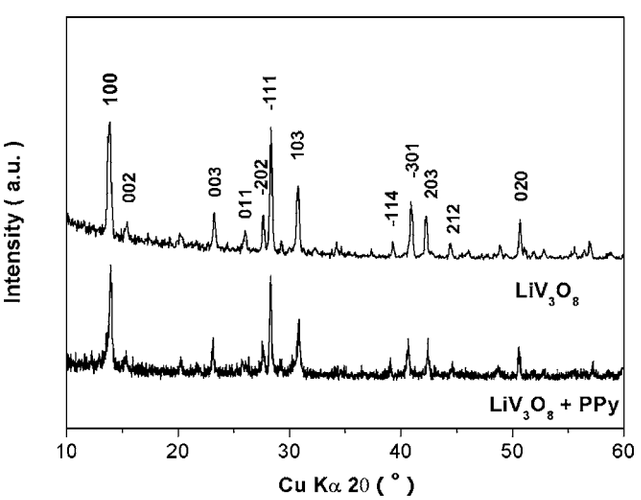

Figure 3. XRD pattern of bare LiV_3O_8 and LiV_3O_8–PPy composite.

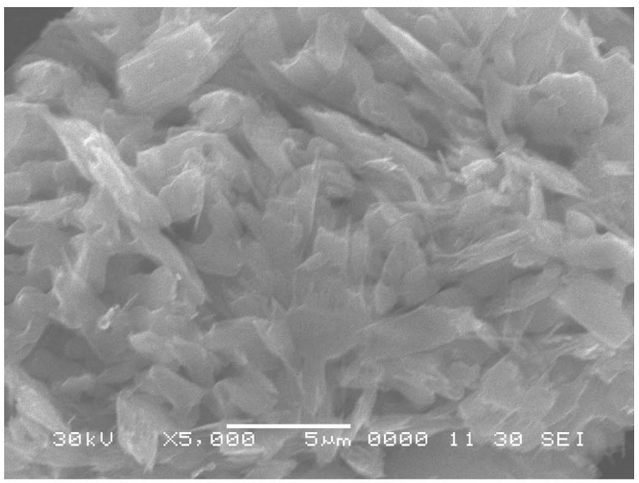

(a)

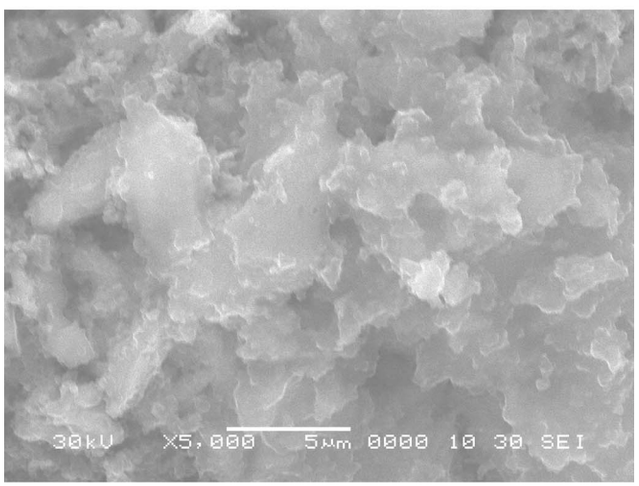

(b)

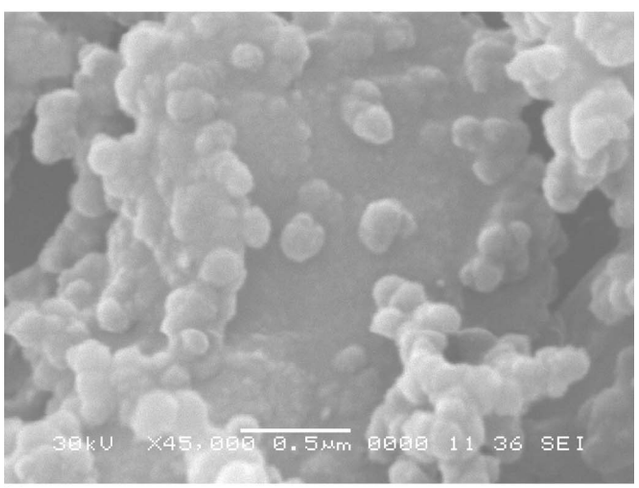

(c)

Figure 4. SEM images of (a) pure LiV_3O_8, (b) LiV_3O_8–PPy composite, and (c) LiV_3O_8–PPy composite at higher magnification.

correspond to the presence of the elements V, N, and C, respectively, in which the N and C are elements of PPy. The results show that N and C are distributed homogeneously throughout the V element, indicating a uniform coating of nano-PPy within the LiV_3O_8 particles. The homogeneity of the nanocomposite plays a fundamental role in terms of cyclability and rate capability.[21,22]

Electrochemical performance of LiV_3O_8–PPy composite.— The electrochemical properties of LiV_3O_8–PPy composites were systematically investigated. Figure 6 summarizes the 10th, 50th, and 100th charge/discharge curves for LiV_3O_8 and LiV_3O_8–PPy composite electrodes. The calculated capacities for both materials were solely based on the active material, LiV_3O_8 particles in the electrode. Even though the discharge capacity of the bare LiV_3O_8 electrode (Fig. 6a) at the 10th cycle was 182 mAh g^{-1}, further cycling led to a rapid capacity decay to 110 mAh g^{-1} (at the 100th cycle), whereas the cycling performance of the LiV_3O_8–PPy composite electrode is better than that of the bare LiV_3O_8 electrode, with a reversible capacity of 183 mAh g^{-1} after the 100th cycle (Fig. 6b).

There are several plateaus in the voltage profiles for the lithium intercalation and deintercalation of the LiV_3O_8 and the LiV_3O_8–PPy composite electrode (as shown in Fig. 6). These voltage plateaus correspond to cathodic/anodic peaks and were translated into the differential capacity curves shown as insets in Fig. 6a and b and Fig. 7. The profiles of the differential curves for both electrodes are nearly identical. The main anodic peaks appear at a potential of about 2.6–2.8 V, which is related to the insertion of Li^+ into LiV_3O_8. And, the cathodic peaks are located at 2.7–2.8 V, which indicates the extraction of Li^+ from LiV_3O_8. The intensity of these peaks in the LiV_3O_8 electrode decreases with cycling (inset in Fig. 6a), especially in the anodic region, indicating poor cycle stability, whereas the peak intensity for the LiV_3O_8–PPy composite electrode remains stable (Fig. 6b) upon cycling. As shown in Fig. 7, at the 50th cycle, the LiV_3O_8–PPy composite electrode shows a higher peak intensity than the LiV_3O_8 electrode, suggesting higher insertion capacity and faster kinetics for Li^+ intercalation/deintercalation in the LiV_3O_8/nano-PPy composite electrode.

The discharge capacities as a function of cycle number are compared in Fig. 8. It was found that the initial capacity of the LiV_3O_8 electrode is higher than that of the LiV_3O_8–PPy composite electrode. The first discharge capacities for bare LiV_3O_8 electrodes are as high as 210 mAh g^{-1}. However, after 50 cycles, the capacity dropped rapidly to 126 mAh g^{-1}. Meanwhile, the first discharge capacity for the LiV_3O_8/nano-PPy composite electrode was 184 mAh g^{-1}. Subsequently, the material was stable, and the capacity remained above 183 mAh g^{-1} beyond 100 cycles. The cycle stability of LiV_3O_8–PPy composite electrode is best proven by the capacity retention curve as shown in Fig. 9. The discharge capacity for the bare LiV_3O_8 electrode after 100 cycles is relatively poor, which is 48% of the initial discharge capacity. In contrast, the LiV_3O_8–PPy composite electrode maintained high activity and excellent reversibility, with a capacity retention of about 98% after 100 cycles.

During cycling, the discharge capacity of the LiV_3O_8–PPy composite first increased, reached a maximum at the 10th cycle, and maintained a stable cycle life of $\sim$183 mAh g^{-1}. The increase in the discharge capacity of the LiV_3O_8–PPy composite at the first 10 cycles is attributed to the increase in the intercalation of Li^+ ions into the composite.[23-25] It is believed that PPy particles are uniformly coated onto the surface of LiV_3O_8 powders, which results in low diffusivity/intercalation of Li^+ ion at the initial stage. After a few cycles, some minor defects were found on PPy particles where more diffusion paths are provided for Li^+ ions to intercalate with LiV_3O_8 particles and, thus, an increase in capacity was observed. To verify this concept, ac impedance measurements were conducted. The Nyquist plots obtained for LiV_3O_8–PPy composite electrode before cycle and after 10 cycles in the fully charged state are compared in Fig. 10. The thickness of the electrodes was about 50 μm with a coated area of 1 cm^2. The diameter of the semicircle for the LiV_3O_8–PPy composite electrode is 135 Ω after 5 cycles and 95 Ω after 10 cycles. The diameters of both semicircles are much smaller

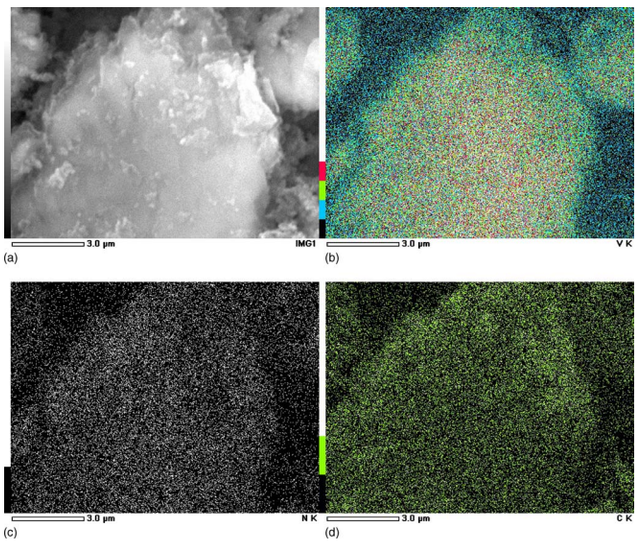

Figure 5. (Color online) EDX mapping of LiV_3O_8–PPy composite: (a) original image, (b) V mapping, (c) N mapping, and (d) C mapping.

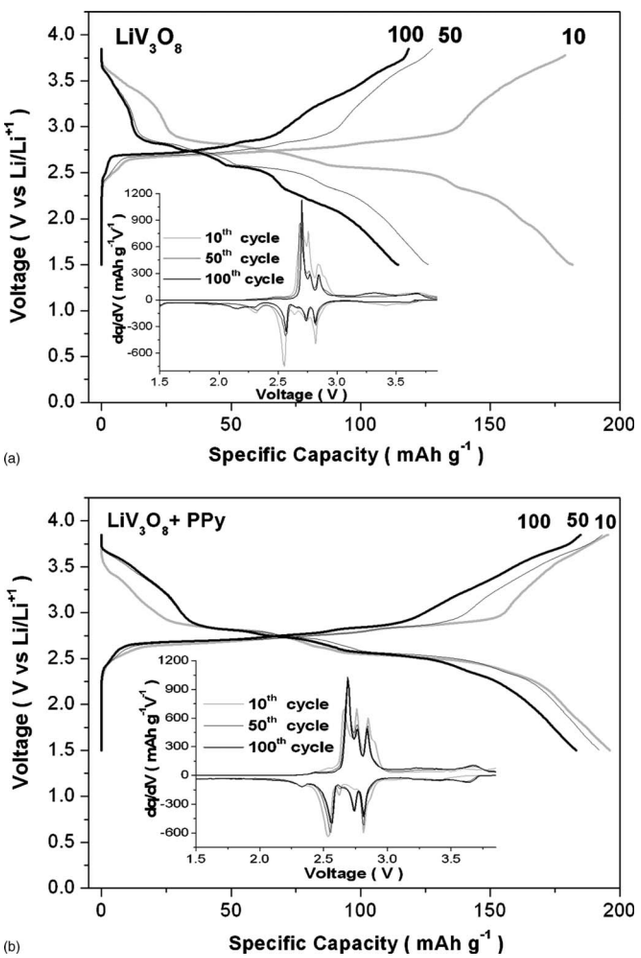

Figure 6. The 10th, 50th, and 100th charge/discharge curves of (a) the bare LiV_3O_8 electrode and (b) the LiV_3O_8–PPy composite electrode (with the number indicating the cycle number). The insets show the corresponding differential capacities.

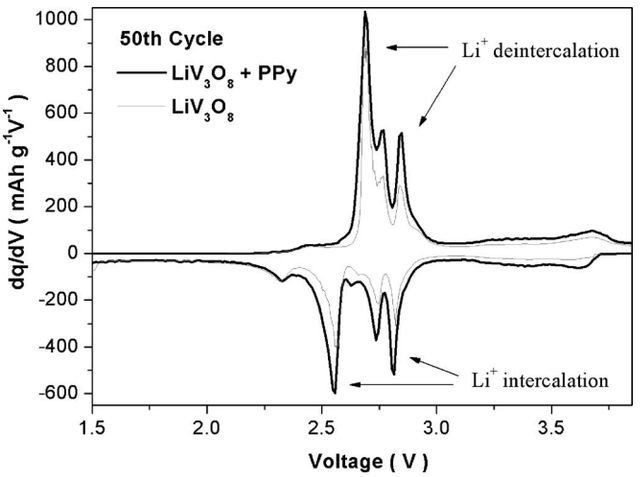

Figure 7. Differential capacity plots for bare LiV_3O_8 and LiV_3O_8–PPy composite at the 50th cycle.

compared with LiV_3O_8–PPy composite electrode before cycle (425 Ω). The diameter of the semicircle represents the interparticle contact resistance.[26] Therefore, it can be assumed that the interparticle resistance was suppressed with the presence of PPy. When the high accessibility of Li^+ ions is coupled with the high electronic conductivity of the PPy, a good cycling performance of the LiV_3O_8–PPy composite electrode is achieved.

The improved cyclability of the LiV_3O_8–PPy composite electrode is verified by analyzing the surface morphology of the electrode after cycling. Figure 11 shows SEM images of both electrodes after 100 cycles. Larger cracks can be clearly observed in the bare LiV_3O_8 electrode compared with the LiV_3O_8–PPy composite electrode, which confirmed that the well-dispersed PPy particles work well as both a conducting matrix and a binder for LiV_3O_8.

Conclusions

PPy-coated LiV_3O_8 composites were successfully synthesized by a low-temperature solution method followed by an in situ polymerization method. The resulting composites exhibit excellent cyclability and high coulombic efficiency, with a specific capacity retention of ~183 mAh g^{-1} after 100 cycles. Our preliminary investigations on PPy composite with different oxides have suggested that PPy works well as a conducting matrix and a binder. More work on

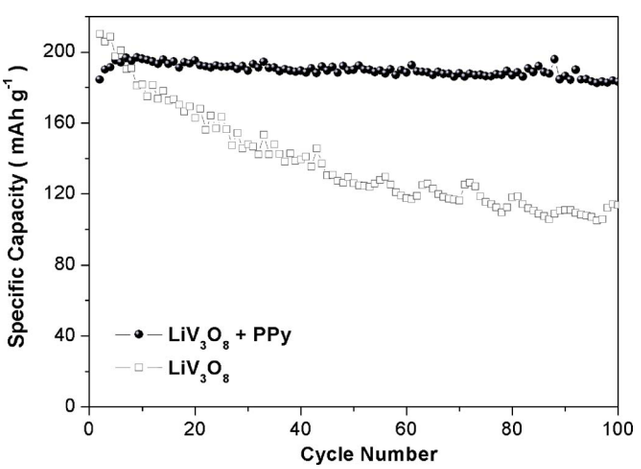

Figure 8. Cycle life of bare LiV_3O_8 and LiV_3O_8–PPy composite.

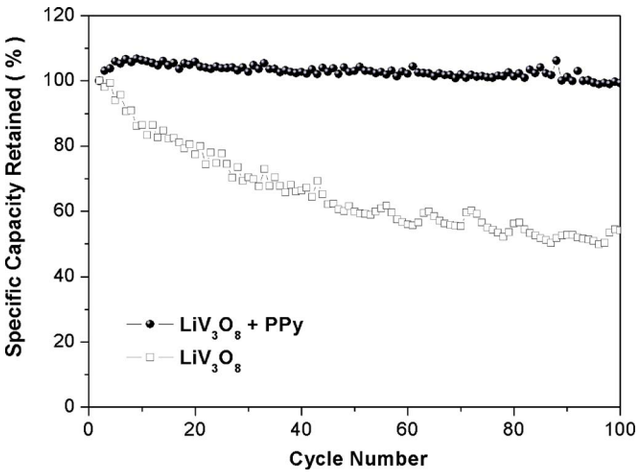

Figure 9. Capacity retention vs cycle number of bare LiV_3O_8 and LiV_3O_8–PPy composite.

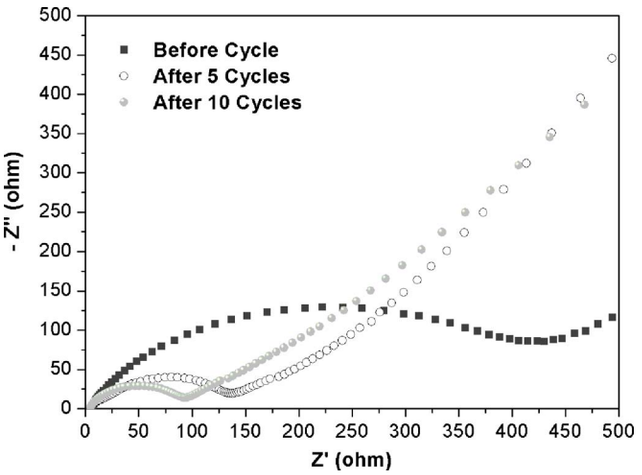

Figure 10. Impedance plots for the LiV_3O_8–PPy composite electrode.

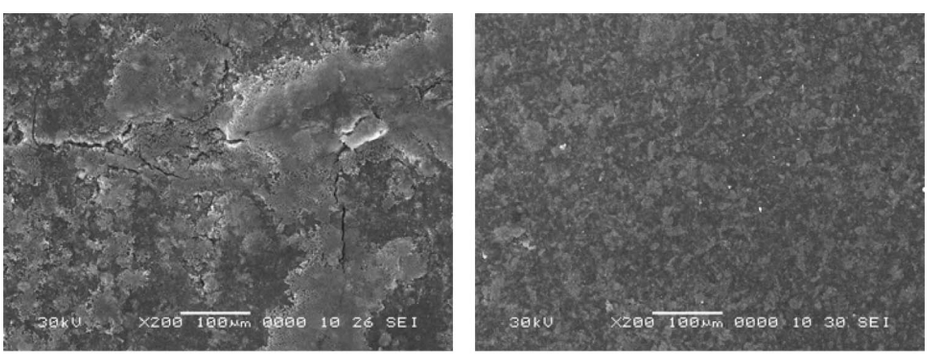

(a) (b)

Figure 11. SEM images of electrodes after 100 cycles: (a) LiV_3O_8 electrode and (b) LiV_3O_8–PPy composite electrode.

LiV_3O_8–PPy composite, with various compositions of PPy, and on its use in rechargeable lithium cells is now in progress.

Acknowledgments

Financial support provided by the Australian Research Council (ARC) through ARC Centre of Excellence funding (CE0561616) is gratefully acknowledged. The authors also thank Dr. Tania Silver at the University of Wollongong for a critical reading of the manuscript.

University of Wollongong assisted in meeting the publication costs of this article.

References

1. J.-M. Tarascon and M. Armand, *Nature (London)*, **414**, 359 (2001).
2. D. Linden, *Handbook of Batteries*, 2nd ed, pp. 36.9–36.12, McGraw-Hill, New York (1995).
3. S. Panero, M. Pasquali, and G. Pistoia, *J. Electrochem. Soc.*, **130**, 1225 (1983).
4. K. Nassau and D. W. Murphy, *J. Non-Cryst. Solids*, **44**, 297 (1981).
5. G. Pistoia, S. Panero, M. Tocci, R. V. Moshtev, and V. Manev, *Solid State Ionics*, **13**, 311 (1984).
6. G. Pistoia, M. Pasquali, G. Wang, and L. Li., *J. Electrochem. Soc.*, **137**, 2365 (1990).
7. M. Dubarry, J. Gaubicher, D. Guyomard, N. Steunou, and J. Livage, *Chem. Mater.*, **16**, 4867 (2004).
8. K. West, B. Zachau-Christiansen, M. J. L. Østergård, and T. Jacobsen, *J. Power Sources*, **20**, 165 (1987).
9. N. Kumagai and A. Yu, *J. Electrochem. Soc.*, **144**, 830 (1997).
10. G. Q. Liu, C. L. Zeng, and K. Yang, *Electrochim. Acta*, **47**, 3239 (2002).
11. H. Y. Xu, H. Wang, Z. Q. Song, Y. W. Wang, H. Yan, and M. Yoshimura, *Electrochim. Acta*, **49**, 349 (2004).
12. G. Yang, G. Wang, and W. Hou, *J. Phys. Chem. B*, **109**, 11186 (2005).
13. H. Yoneyama, A. Kishimoto, and S. Kuwabata, *J. Chem. Soc., Chem. Commun.*, **1991**, 986.
14. A. H. Gemeay, H. Nishiyama, S. Kuwabata, and H. Yoneyama, *J. Electrochem. Soc.*, **142**, 4190 (1995).
15. H. P. Wong, B. C. Dave, F. Leroux, J. Harreld, B. Dunn, and L. F. Nazar, *J. Mater. Chem.*, **8**, 1019 (1998).
16. J. Wang, J. Chen, K. Konstantinov, L. Zhao, S. H. Ng, G. X. Wang, Z. P. Guo, and H. K. Liu, *Electrochim. Acta*, **51**, 4634 (2006).
17. G. X. Wang, L. Yang, Y. Chen, J. Z. Wang, S. Bewlay, and H. K. Liu, *Electrochim. Acta*, **50**, 4649 (2005).
18. P. Novák, K. Müller, K. S. V. Santhanam, and O. Haas, *Chem. Rev. (Washington, D.C.)*, **97**, 207 (1997).
19. J. Kawakita, T. Miura, and T. Kishi, *Solid State Ionics*, **120**, 109 (1999).
20. L. A. de Picciotto, K. T. Adendorff, D. C. Liles, and M. M. Thackeray, *Solid State Ionics*, **62**, 297 (1993).
21. J. M. Chabagno, D. Deroo, F. Dalard, and J. L. Merienne, *Solid State Ionics*, **13**, 45 (1984).
22. G. Pistoia, M. Pasquali, Y. Geronov, V. Manev, and R. V. Moshtev, *J. Power Sources*, **27**, 35 (1989).
23. J. Dai, S. F. Y. Li, Z. Gao, and K. S. Siow, *J. Electrochem. Soc.*, **145**, 3057 (1998).
24. Y. Huang, K. Park, and J. B. Goodenough, *J. Electrochem. Soc.*, **153**, A2282 (2006).
25. S. Kuwabata, S. Masui, H. Tomiyori, and H. Yoneyama, *Electrochim. Acta*, **46**, 91 (2000).
26. J. Fan and P. S. Fedkiw, *J. Power Sources*, **72**, 165 (1998).